Vibrational Frequencies of the 2p $^2A_2''$ and 3d $^2E''$ States of the Triatomic Deuterium Molecule

U. Müller, M. Braun, R. Reichle, and R. F. Salzgeber
Universität Freiburg, Fakultät für Physik,
Hermann-Herder-Str. 3, D-79104 Freiburg, Germany

February 2, 2008

Abstract

We investigated the vibrational energies in the 2p $^2A_2''$ and 3d $^2E''$ states of the triatomic deuterium molecule D_3. The experiments were performed using a fast neutral beam photoionization spectrometer recently developed at Freiburg. A depletion type optical double-resonance scheme using two pulsed dye lasers was applied. The measured vibrational frequencies of the 2p $^2A_2''$ state of D_3 are compared to those of H_3 and to theoretical values calculated from an *ab initio* potential energy surface. The data give insight into the importance of the coupling between the valence electron and the ion core.

PACS-Numbers: 33.80.Rv, 33.20.Kf, 33.20.Lg, 34.10.+x, 34.30.+h

1 Introduction

The triatomic hydrogen molecule, the simplest neutral polyatomic molecule, is ideally suited to study fundamental aspects of the interaction between the electronic and the nuclear motion. The molecule is sufficiently small for high precision *ab initio* investigations of the potential energy surfaces to be successful [1, 2]. Excited states of H_3 and D_3 were discovered by Herzberg and coworkers [3, 4, 5, 6] in emission from electrical gas discharges in hydrogen and deuterium. All of the excited states are predissociated by coupling to the repulsive ground state potential energy surface except for the single rotational state 2p $^2A_2''$(N=K=0) which is metastable and can be prepared in a fast neutral beam by charge transfer of H_3^+ or D_3^+ [7, 8, 9, 10] in cesium. The H_3 2p $^2A_2''$(N=K=0) state was used as a platform for laser-excitation/ionization experiments in order to explore the Rydberg states of H_3 and to determine their vibrational frequencies [7, 11, 12, 13, 14, 15, 16, 17] .

In a recent investigation from this laboratory [18], we created a fast beam of rotationless D_3 molecules in the lowest vibrational levels of the 2p $^2A_2''$ metastable state. Following vibrationally diagonal excitation in the ultraviolet spectral range, we observed five Rydberg series. Two series were detected by field-ionization and assigned to s– and d– type Rydberg states with a vibrationless D_3^+ core. Three series were found to consist of transitions from vibrationally symmetric stretch and degenerate mode excited 2p $^2A_2''$ states into auto-ionizing Rydberg states. In order to assign the core vibrational excitation, we used preliminary results of a depletion type double resonance experiment. A vibrationally non-diagonal transition which appears as a Fano type line above the first ionization limit allowed us to determine the first symmetric stretch vibrational frequency of the D_3 2p $^2A_2''$ state. In order to determine the degenerate mode frequency of the 2p $^2A_2''$ state, we used the molecular constants of the D_3^+ ion[19].

The objectives of the present investigation are threefold. First, we present the results of double resonance experiments which confirm the assignment of the Rydberg states observed previously [18]. Secondly, we investigate vibrationally diagonal and non-diagonal transitions from the 2p $^2A_2''$ state to vibrationally ground and exited levels of the 3d $^2E''$ state. In this way, we determine the vibrational frequencies of the 2p $^2A_2''$ and 3d $^2E''$ states of D_3. Third, we calculate the vibrational levels of the 2p $^2A_2''$ states of H_3 and D_3 with the potential energy surface published recently by Peng et al. [2]

using the filter diagonalization method in the version of Mandelshtam and Taylor [20]. The comparison between the experimental data and the theoretical model gives insight into the influence of the Rydberg electron on the bond strength. By using different isotopes, the potential energy surface is effectively probed.

2 Experimental

In this study, we used the fast beam collinear spectrometer recently developed at Freiburg [18]. Triatomic deuterium ions (D_3^+) were created in a hollow cathode discharge in deuterium (D_2). The cathode was cooled by liquid nitrogen. The ions were accelerated to an energy of 3.6 keV and mass selected by a Wien-filter. A small fraction of the ions was neutralized by charge transfer in cesium vapor. After the charge-transfer cell, the unreacted ions were removed by an electric field. A 1 mm diameter aperture located 30 cm downstream of the charge transfer cell was used to stop products of dissociative charge transfer. Fast metastable molecules which entered the 120 cm long laser-interaction region were excited by a counterpropagating pulsed dye laser beam. Photoions were detected at the end of the interaction region by an energy analyzer and a microsphere plate. A 200 MHz dual-counter was used to accumulate the signal produced by the laser pulses and the background events separately. The data were then transferred to a laboratory computer and stored for further treatment.

In order to perform depletion type double resonance experiments, we operated two dye lasers pumped by an excimer laser. The wavelengths of both dye lasers were programmed and/or scanned under control of the laboratory computer. Using an optical delay line, the pulses of one of the dye lasers (labelling laser) were delayed by about 15 ns with respect to the pulses of the other dye laser (excitation laser). Both laser beams were merged by a beamsplitter before they entered the interaction region. The labelling laser was operated at a fixed wavelength, and used to excite a transition from a specific vibrational level of the 2p $^2A_2''$ state to a field- or autoionizing state. The ion signal was used to monitor the population in the lower state. The excitation laser was scanned in the tuning ranges of the dyes Rhodamine 6G and Coumarin 307. Transitions originating from the labelled lower state lead to a reduction of the ion signal and appear as depletion dips in the spectra. The depletion technique is most effective in the case of transitions to upper states which are quickly predissociated. A long-lived upper

state may be ionized by a second photon from the same excitation laser pulse (1+1 REMPI) which reduces the depth of the depletion feature. In that case, the intensity of the excitation laser was reduced by neutral density filters.

In order to calibrate the wavelength scales of the lasers, the optogalvanic signal from a hollow cathode discharge in neon and argon was recorded, and the observed lines were compared to tabulated values [22]. The Rank-formula [23] was used to correct for the refractive index of air. The Doppler-shift due to the motion of the fast neutral molecules was calculated from the acceleration voltage of the ion source. We estimate the systematic uncertainty of the photon energy scale to be less than 0.2 cm^{-1}.

3 Numerics

The significance of any molecular eigenstate calculation, depends strongly on the quality of the potential energy surface (PES) on which it is performed. For computing the low lying vibrational frequencies of H_3 and D_3 in the 2p $^2A_2''$ state, we use the fitted *ab initio* potential energy surface of Peng et al.[2]. This seems to be a rather accurate fit (with only 5 cm^{-1} average deviation from its 1340 *ab initio* points [2]), thus enabeling us to make a rather precise prediction of its eigenstates.

¿From the various methods for computing vibrational states of small molecular systems, we use the low-storage version of the filter-diagonalization method introduced recently by Mandelshtam and Taylor [20]. This method is conceptually based on the filter-diagonalization procedure of Wall and Neuhauser [24] which extracts the system eigenenergies by harmonic inversion of a time correlation function C(t). The method of ref. [20] is designed to use a direct harmonic inversion of the Chebyshev correlation function [21]

$$c_n = \langle \xi_0 | T_n(\hat{H}) | \xi_0 \rangle \sim \sum_k d_k \cos n\omega_k \ , \tag{1}$$

for the eigenenergies $E_k = \cos\omega_k$ and amplitudes d_k. The computation of the c_n sequence is done to essentially the machine precision using a very inexpensive iterative numerical scheme,

$$\xi_1 = \hat{H}\xi_0, \ \ldots \ , \ \xi_{n+1} = 2\hat{H}\xi_n - \xi_{n-1} \ , \tag{2}$$

with c_n being generated using $c_{2n} = 2\langle \xi_n | \xi_n \rangle - c_0$, $c_{2n-1} = 2\langle \xi_{n-1} | \xi_n \rangle - c_1$. This requires to store only a few vectors at a time, if the matrix-vector multiplication is implemented

without explicit storage of the Hamiltonian matrix. The spectral analysis part (i.e., the harmonic inversion of c_n by the filter-diagonalization) is carried out independently and efficiently after the sequence c_n is computed. All these features imply the very high performance of the overall numerical procedure.

It is not hard to achieve a precision of the low lying states of $\Delta E/E = 10^{-4}$, because their density of states is not high, and, therefore, the number of iterations can be small ($\sim 10^3$), requiring only a few hours of CPU time on a RS6000/59H workstation.

We choose Radau coordinates, in which all mixed derivatives in the kinetic energy vanish [25], to guarantee for a fast application of the Hamiltonian to a vector, which is the bottleneck in iterative methods. However, this choice of coordinates implies that C_{2v} symmetry, rather than the full D_{3h} symmetry of H_3 (D_3), is used in the calculation. Nevertheless, E states can be identified as a numerically close pair of an A' and an A'' state [26].

We also use a sinc-DVR [27] for the radial and a Legendre-DVR for the angular part of the Hamiltonian. The parameters defining the grid are the size of the primitive sinc-basis $n_1 = n_2$, which are truncated by a kinetic energy cutoff to $n_{1b} = n_{2b}$, their spatial extension from $r_{i\,min}$ to $r_{i\,max} (i = 1, 2)$, the size of the primitive basis of the Legendre polynomials for the angular motion n_3 and a three-dimensional potential energy cutoff V_{cut}. All primitive basis parameters have been adjusted in the one-dimensional problem, with the remaining coordinates held fixed to their equilibrium values. The details of the convergence procedure will be described in [28].

For H_3 we used the values $n_1 = n_2 = 71, n_{1b} = n_{2b} = 60, n_3 = 67, V_{cut} = 13.06eV$ above the minimum of the potential, and $r_{1\,min} = r_{2\,min} = 0.7a_0, r_{1\,max} = r_{2\,max} = 7.1a_0$, overall resulting in 232 705 gridpoints. The figures for D_3 were $n_1 = n_2 = 49, n_{1b} = n_{2b} = 43, n_3 = 67, V_{cut} = 12.06eV$ above the minimum of the potential, and $r_{1\,min} = r_{2\,min} = 0.8a_0, r_{1\,max} = r_{2\,max} = 4.2a_0$, resulting in 116 192 gridpoints.

The results, which are shown in table 3, have an accuracy of better than 0.25 cm^{-1} assuming the PES is correct, which e.g. follows from comparison of the A' and A'' components of the E states. Additionally, convergence was ensured by running various grids of increasing size.

4 Results and Discussion

In Table 1, the ionization limits and quantum defects of five Rydberg series detected in a previous investigation from this laboratory [18] are listed. Series 1 and 2 were observed by field-ionization and assigned to d- and s-type Rydberg series, respectively, converging to a vibrationless $D_3^+(N^+ = 1, K^+ = 0)$ state. Series 3 to 5 were found to arise from autoionizing states which are built on vibrationally excited D_3^+ ion cores. We also observed a Fano type resonance at 29652.6 cm^{-1} in the continuum above the first ionization limit of the vibrationless 2p $^2A_2''$ state. In the present investigation, the depletion technique is used in order to decide which transitions share a common lower state, and to determine vibrational frequencies in a straightforward way.

4.1 Depletion measurements of the vibrationless 2p $^2A_2''$ state

With the labelling laser set to a member (n=39) of the field-ionizing series 1, we observed a depletion dip centered at a frequency of 17333.3 cm^{-1}(Fig. 1a). This transition was observed in emission by Herzberg's group and assigned to the 2p $^2A_2''(0,0,0,0) \leftarrow$ 3d $^2E''(0,0,1,0)$ transition of D_3[6]. We describe the rovibrational states by the set (ν_1,ν_2,N, G) with the quantum numbers of the symmetric stretch (A_1') and the degenerate mode (E') vibrations ν_1 and ν_2, the total angular momentum apart from spin N, and Hougen's convenient quantum number $G = l + \lambda - K$ [29], which contains the projections of the total (K), the electronic (λ), and the vibrational angular momentum (l) onto the figure axis. The depletion feature in Fig. 1a shows clearly that the vibrationless 2p $^2A_2''(0,0,0,0)$ state is the lower state of Rydberg series 1 and 2. The large width of 0.8 cm^{-1} is mainly due to power-broadening . The depletion in the center of the dip is almost complete which indicates a strong decay mechanism of the upper state either by predissociation or by radiation into a state different from 2p $^2A_2''(0,0,0,0)$.

We scanned the excitation laser in the tuning range of Coumarin 307, and observed in a 300 cm^{-1} wide region a single depletion dip centered at 19629.4 cm^{-1} (labelling by n=40 of series 1, Fig.1b). The width of the dip is about 0.2 cm^{-1} FWHM. The difference between the locations of the depletion features shown in Fig.1 is 2296.1 cm^{-1}. This value is extremely close to the 2300.843 cm^{-1} symmetric stretch vibrational frequency of the D_3^+ ion [19]. We, therefore, assign the upper state of the transition at 19629.4

cm^{-1} to the vibrationally symmetric stretch excited 3d $^2E''(1,0,1,0)$ state. The Franck-Condon factor of this vibrationally non-diagonal transition is quite small. Therefore, the transition to the 3d $^2E''(1,0,1,0)$ state (Fig. 1b) is much less power-broadened than that to the 3d $^2E''(0,0,1,0)$ state (Fig. 1a). The depletion depth in Fig. 1b is about half of the ion signal. With the exitation laser (Coumarin 307) unattenuated and the ionization laser blocked, we observe a strong REMPI peak at 19629.4 cm^{-1}. Both observations are in line with a comparatively long natural lifetime of the vibrationally excited 3d $^2E''$ state.

With the labelling laser tuned to the peak of the Fano type resonance at 29652.6 cm^{-1}, we observe depletion centered at 19629.4 cm^{-1}(Fig 2a,b). The depth is about half of the steady ion signal which demonstrates that the Fano type feature is quantitatively depleted. The measurements presented in Figs. 1 and 2 demonstrate that the lines of series 1 and 2, the transitions to the vibrationally ground and symmetric stretch excited 3d $^2E''$ states at 17333.3 and 19629.4 cm^{-1}, respectively, and the Fano-type peak at 29652.6 cm^{-1} originate from the vibrationless 2p $^2A_2''(0,0,0,0)$ metastable state of D_3. These transitions are shown in the level scheme Fig. 7 with the common lower state labelled by I.

4.2 Depletion measurements of vibrationally excited 2p $^2A_2''$ states

The objective is to determine the core excitation of the autoionizing d– and s–Rydberg states of series 3 and 4 converging to a limit of 29535.1 cm^{-1}, and the d–states of series 5 converging to 29547.8 cm^{-1}. In Fig. 3, vibrationally diagonal transitions to autoionizing states in the 27230 cm^{-1} to 27350 cm^{-1} and the 27760 cm^{-1} to 27840 cm^{-1} energy range are shown. The positions of the n=7 and n=8 lines of series 3 to 5 calculated from the series limits and quantum defects in Table 1 are indicated by the open circles in Figure 3. As discussed previously [18], the thresholds for vibrational autoionization of Rydberg states calculated from the molecular constants of D_3^+ [19] are n=8 and n=7 for a core excitation of one quantum in the degenerate and symmetric stretch mode, respectively. This should allow us to determine the core excitation of the different series from the lowest observed principal quantum number lines. The peaks F, D and G are the n=8 members of series 3,4, and 5, respectively. In the n=7 range, the assignment is not unique. Peak B corresponds to n=7 of series 5. Peak A could

belong to series 4. The peak C cannot be assigned to any of the series in Table 1.

Therefore, we performed depletion experiments with the labelling laser tuned to the peaks A to G, and the excitation laser operating with Rhodamine 6G. The results are presented in Figs. 4 and 5. Labelling the peaks A,B,C, E, and G we found depletion dips at 17264.5 cm^{-1}. On the other hand, labelling the peaks D and F, we clearly observed dips at 17270.5 cm^{-1}. We cross-checked and found that the lines D and F and the lines A,B,C, E, and G are excited from the common lower states II and III, respectively, as shown in the level scheme Fig. 7 . None of the features in the left part of Fig. 3 arises from state II. The peaks D and F are the lowest principal quantum number lines of series 3 and 4 and the autoionization threshold of these series is n=8. It follows that the ion cores of the Rydberg states of series 3 and 4 and of the common lower state (II in Fig. 7) are in the first degenerate mode excited vibrational state (ν_1=1, ν_2=2). The assignment of the peaks A, C, and E in Fig. 3 will be discussed below.

In the measurement presented in Fig. 6, peak G (n=8 of series 5) was excited by the labelling laser and the excitation laser was tuned in the 17256 cm^{-1} to 17285 cm^{-1} range. In spectrum (a) of Fig. 6, the pulse energy of the excitation laser was 120 μJ. Spectra (b) and (c) of Fig. 6 were recorded with the excitation laser attenuated by factors of 10 and 20 respectively using neutral density filters. We observe two depletion features at 17264.5 cm^{-1} and at 17276.1 cm^{-1} respectively. At high pulse energy of the excitation laser, the feature at 17264.5 cm^{-1} is comparatively narrow and in the center of the dip, the ion signal is almost completely depleted. This feature disappears at low pulse energy. The dip at 17276.1 cm^{-1} appears broad and shallow with a width of about 1 cm^{-1} FWHM at high pulse energy. At a laser energy as low as 6 μJ, the depletion of the ion signal is almost complete and the width is reduced by a factor of 3 to about 0.3 cm^{-1}. This shows that the transition moment of the line at 17276.1 cm^{-1} is by at least one order of magnitude stronger than that of the line at 17264.5 cm^{-1}.

4.3 Symmetric Stretch Frequency of the D_3 2p $^2A_2''$ State

In the level scheme Fig. 7, the transitions which were found by the depletion technique to originate from the lower states labelled by I, II, and III are indicated by vertical lines. As already discussed, state I was identified to be the vibrationless metastable

state 2p $^2A_2''(0,0,0,0)$. State II was found to be the degenerate mode (E′) excited 2p $^2A_2''$ state. We notice that the difference between the Fano-type feature at 29652.6 cm^{-1} and the 2p $^2A_2''(0,0,0,0)\rightarrow$3d $^2E''(1,0,1,0)$ transition at 19629.4 cm^{-1} is 10023.2 cm^{-1}. This value is in (almost too) perfect agreement with the difference between the transitions at 27299.3 cm^{-1} (peak B in Fig. 3) and at 17276.1 cm^{-1} (Fig. 6) both originating from state III . We do not find any other combination differences between the observed transitions which would coincide within the experimental accuracy. This leads us to conclude that the upper states connected by the dashed horizontal lines in Fig. 7 are identical. As a consequence, the separation between the states I and III calculated via the 3d $^2E''(1,0,1,0)$ intermediate state is found to be 2353.3 cm^{-1}. This value is extremely close to the first symmetric stretch vibrational frequency of the D_3^+ ion. We conclude that state III is the symmetric stretch excited 2p $^2A_2''(1,0,0,0)$ state. It follows that the previous assignment [18] of series 5 to converge to a symmetric stretch excited D_3^+ state is correct.

In order to assign the peaks A, C, and E we calculated the principal quantum numbers and quantum defects of all the features in Fig. 3 which were found to have the symmetric stretch excited 2p $^2A_2''(1,0,0,0,)$ state as the lower state. We used the 29547.8 cm^{-1} limit of series 5 which converges to a symmetric stretch excited D_3^+ state. The values are listed in Table 2. The peaks B and G with n=7, δ =0.0143 and n=8, δ =0.0138 respectively have already been recognized to be d states of series 5 and are listed for completeness in Table 2. Based on the quantum defect of δ=0.060, peak E is assigned to the 8s state with symmetric stretch excited core.

The quantum defect δ=0.092 of peak A is significantly larger than the typical values for s–states (c.f. tab. 1) and we have to understand the peak width of 3 cm^{-1} FWHM which is appreciably larger than that of the other features in Fig. 3. The peak center at 27248.7 cm^{-1} is extremely close to the energy difference of 27247.7 cm^{-1} between the symmetric stretch excited 2p $^2A_2''(1,0,0,0)$ state and the first ionization limit of the vibrationless 2p $^2A_2''(0,0,0,0)$ ground state. Transitions between the 2p $^2A_2''(1,0,0,0)$ state and the vibrationless s– and d– states of series 1 and 2 are optically allowed, but the Franck-Condon factors are very small. Feature A could arise from an interference between the vibrationally diagonal transition from the 2p $^2A_2''(1,0,0,0)$ state to the symmetric stretch excited 7s state and non-diagonal transitions to vibrationless high

principal quantum number s– and d– states of series 1 and 2.

Based on the quantum defect of δ=-0.002, peak C was explained in a previous study [18] by an interloper of a g–series with symmetric stretch excited core. Another explanation is a vibrationally non-diagonal transition to a 5s (2,0,1,0) state with two quanta of excitation in the symmetric stretch mode. The series limit listed in Table 2 was calculated from the molecular constants of D_3^+ determined by Amano et al. [19]. The quantum defect of δ=0.0566 is in line with the values generally observed for low principal quantum number s–states.

4.4 Comparison between Experimental and Theoretical Results

In Table 3, the energies of the lowest vibrational states of H_3 2p $^2A_2''$ and D_3 2p $^2A_2''$ determined by theoretical and experimental investigations are listed. The values are given relative to the vibrationless states. The theoretical data are calculated from the *ab initio* potential energy surface by Peng et al.[2] using the procedure described in Section 3. For comparison, the vibrational frequencies of the H_3^+ and D_3^+ ions determined by Majewski et al. [30] and by Amano et al. [19] are included in Table 3. The differences between the vibrational frequencies of the neutrals and the ions are quite large which shows the valence character of the 2p $^2A_2''$ state. The use of *ab initio* potential energy surfaces is mandatory in order to calculate the vibrational levels to a satisfactory accuracy. A treatment based on a quantum defect, which is independent of the nuclear coordinates, is condemned to fail. The experimental results for D_3 were measured in this and in a previous investigation from this laboratory [18], and the data for H_3 were taken from Ketterle et al. [14]. The value of 3255.4 cm^{-1} for the symmetric stretch frequency of the H_3 2p $^2A_2''$ state measured by Lembo and Helm [16] is in close agreement with the value of 3255.38 cm^{-1} measured by Ketterle et al. [14]. The uncertainties of the experimental data which are estimated to be $\pm$0.3 cm^{-1} for D_3 and $\pm$0.1 cm^{-1} for H_3, are generally much smaller than the differences between experiment and theory which are of the order of a few cm^{-1}, the largest being 6.6 cm^{-1} in case of the E′– vibration of H_3 2p $^2A_2''$. As discussed above, the numerical procedure for the calculation of the eigenvalues is converged to an accuracy better than 0.25 cm^{-1}. Therefore, the differences between experiment and theory must be attributed to the potential energy surface which was fitted to the *ab initio* points with an average

deviation of 5 cm^{-1} and a root mean square deviation of 170 cm^{-1} [2]. The shape of the fitted PES in the region occupied by the low vibrational states is apparently quite good. The observed differences between the vibrational frequencies of the neutrals and the ions are in very good agreement with the theoretical data as visualized in Fig. 8 where we present the differences between the vibrational frequencies of the 2p $^2A_2''$ states and those of the corresponding ions, normalized to the frequencies of the ions for easier comparison. The measured symmetric stretch frequencies of the 2p $^2A_2''$ states of D_3 and H_3 are roughly 2 % higher than those of the D_3^+ and H_3^+ ions, respectively, which is very well reproduced by the calculated data. In the case of the degenerate mode vibration, the relative differences between neutrals and ions are almost twice as large. This additional resistance against asymmetric deformation induced by the $2p_z$–electron is explained by the theoretical data, although the total effect is slightly underestimated.

5 Conclusions

We investigated the vibrational frequencies of the 2p $^2A_2''$ metastable state and the 3d $^2E''$ state of the triatomic deuterium molecule D_3 by a depletion type double resonance technique. We found a separation of 2296.1 cm^{-1} between the vibrationless D_3 3d $^2E''(0,0,1,0)$ and the symmetric stretch excited 3d $^2E''(1,0,1,0)$ state. The 2353.3 cm^{-1} symmetric stretch frequency of the 2p $^2A_2''$ state determined in a previous investigation from this laboratory was confirmed. We compared the experimental results of the 2p $^2A_2''$ state of D_3 and H_3 with theoretical data calculated from an *ab initio* potential energy surface. The theoretical data describe very well the differences between the vibrational frequencies of the ions and the neutrals which demonstrates the quality of the *ab initio* potential energy surface.

6 Acknowledgements

We are greatly indebted to Prof. H. Helm and Prof. Ch. Schlier for their support, for continuous encouragement during the course of this work, and for critical reading of the manuscript. Thanks must go to S. Kristyan for providing us with the fitted potential energy surface. It is a pleasure to acknowledge technical assistance by U.

Person during the construction and operation of the apparatus. This research was financially supported by Deutsche Forschungsgemeinschaft through its SFB 276.

References

[1] Ch. Nager and M. Jungen, Chem. Phys.**70**, 189 (1982)

[2] Z. Peng, S. Kristyan, A. Kuppermann, and J. S. Wright, Phys. Rev. A. **52**, 1005 (1995)

[3] I. Dabrowski and G. Herzberg, Can. J. Phys. **58**, 1238 (1980)

[4] G. Herzberg and J. K. G. Watson, Can. J. Phys. **58**, 1250 (1980)

[5] G. Herzberg, H. Lew, J. J. Sloan, and J. K. G. Watson, Can. J. Phys. **59**, 428 (1981)

[6] G. Herzberg, J. T. Hougen, and J. K. G. Watson, Can. J. Phys. **60**, 1261 (1982)

[7] H. Helm, L. J. Lembo, P. C. Cosby, and D. L. Huestis, Fundamentals of Laser Interactions II, Lecture Notes in Physics (Ed. F. Ehlotzky), Springer (1989), p. 264

[8] F. M. Devienne, C. R. Acad. Sci. Paris B **267**, 1279 (1968) and **268**, 1303 (1969)

[9] G. I. Gellene and R. F. Porter, J. Chem. Phys. **79**, 5975 (1983)

[10] J. F. Garvey and A. Kuppermann, Chem. Phys. Lett. **107**, 491 (1984)

[11] H. Helm, Phys. Rev. Lett. **56**, 42 (1986)

[12] H. Helm, Phys. Rev. A **38**, 3425 (1988)

[13] A. Dodhy, W. Ketterle, H.-P. Messmer, and H. Walther, Chem. Phys. Lett. **151**, 133 (1988)

[14] W. Ketterle, H.-P. Messmer, and H. Walther, Europhys. Lett. **8**, 333 (1989)

[15] L. J. Lembo, A. Petit, and H. Helm, Phys. Rev. A**39**, 3721 (1989)

[16] L. J. Lembo and H. Helm, Chem. Phys. Lett. **163**, 425 (1989)

[17] L. J. Lembo, D. Huestis, and H. Helm, J. Chem. Phys. **90**, 5299 (1989)

[18] U. Müller, U. Majer, R. Reichle, and M. Braun, JCP **106**, 7958 (1997)

[19] T. Amano, M.-C. Chan, S. Civis., A. R. W. McKellar, W. A. Majewski, D. Sadovskii, and J. K. G. Watson, Can. J. Phys. **72**, 1007 (1994)

[20] V. A. Mandelshtam and H. S. Taylor, J. Chem. Phys. **106**, 5085 (1997).

[21] H. Tal-Ezer and R. Kosloff, J. Chem. Phys. **81**, 3967 (1984).

[22] MIT Wavelength Tables, G. R. Harrison, Cambridge (1969)

[23] D. H. Rank in Advances in Spectroscopy I, ed. H. W. Thompson, New York (1959)

[24] D. Neuhauser and M. Wall, J. Chem. Phys. **102**, 8011 (1995).

[25] B. T. Sutcliffe and J. Tennyson, Intern. J. Quantum Chemistry **39**, 183 (1991).

[26] J. Tennyson and B. T. Sutcliffe, Mol. Phys. **56**, 1175 (1985).

[27] D. T. Colbert and W. H. Miller, J. Chem. Phys. **196**, 1982 (1992).

[28] R. F. Salzgeber, V. A. Mandelshtam, Ch. Schlier, and H. S. Taylor, 1997, to be submitted.

[29] J. T. Hougen, J. Chem. Phys. **37**, 1433 (1962).

[30] W. A. Majewski, A. R. W. McKellar, D. Sadovskii, and J. K. G. Watson , Can. J. Phys. **72**, 1016 (1994)

7 Tables

Table 1: Rydberg series observed following laser-photoexcitation of metastable D_3 2p $^2A_2''$ molecules.

Nr.	$E_{lim}[cm^{-1}]$ [a]	δ	observed n	2p $^2A_2''$ [b]	upper state [b]
1	29601.0	0.015(8)	20-80	(0,0,0,0)	nd1 (0,0,1,0)
2	29601.0	0.08(1)	22-31	(0,0,0,0)	ns1 (0,0,1,0)
3	29535.1	0.014(1)	8-71	(0,1,0,1)	nd1 (0,1,1,1)
4	29535.1	0.07(6)	8-31	(0,1,0,1)	ns1 (0,1,1,1)
5	29547.8	0.015(1)	7-46	(1,0,0,0)	nd1 (1,0,1,0)

[a] The statistical uncertainty of the fit procedure is smaller than the 0.2 cm^{-1} systematic uncertainty of the wavelength calibration

[b] The notation for the rovibrational state is (ν_1,ν_2,N,K)

Table 2: Assignment of the peaks in fig. 7 .

Peak	position	core vibration	E_{lim}	n	δ
A	27248.3	(1,0)	29547.8[a]	7	0.092
B	27299.3	(1,0)	29547.8[a]	7	0.0143
C	27309.8	(1,0)	29547.8[a]	7	-0.0021
E	27807.3	(1,0)	29547.8[a]	8	0.0600
G	27827.4	(1,0)	29547.8[a]	8	0.0138
C	27309.8	(2,0)	31800.0[b]	5	0.0566

[a] Series limit of series 5 in table 1

[b] (ν_1= 2, ν_2=0) ionization limit with respect to the 2p $^2A_2''$(ν_1= 1, ν_2=0) state of D_3 calculated from the ionization limit of series 5 and the molecular constants of D_3^+ [19].

Table 3: Vibrational Energies of the 2p $^2A_2''$ states of H_3 and D_3 compared to those of the corresponding ions.

vib.	H_3^+	$H_3$2p $^2A_2''$				D_3^+ [e]	$D_3$2p $^2A_2''$			
state[a]	ion[b]	th. [c]	th.-ion	exp. [d]	exp.-th.	ion [e]	th. [c]	th.-ion	exp. [f]	exp.-th.
$(0,1)^1$	2521.416	2611.7	90.3	2618.34	6.6	1834.674	1898.8	64.1	1900.9	2.1
$(1,0)^0$	3178.177	3257.6	79.4	3255.38	-2.2	2300.843	2353.3	52.5	2353.3	0.0
$(1,1)^1$	4778.228	4951.9	173.7			3530.385	3650.1	119.7		
$(0,2)^0$	4997.920	5181.5	183.6			3650.658	3777.1	127.1		
$(0,2)^2$	5554.029	5734.1	180.0			4059.470	4182.2	122.7		
$(2,0)^0$	6262.213	6426.6	164.4			4553.792	4661.6	107.8		

[a] the vibrational states $(\nu_1,\nu_2)^l$ are labelled by the number of quanta in the symmetric stretch mode ν_1, the degenerate mode ν_2, and the vibronic angular momentum l. The energy of the vibrationless $(0,0)^0$ state was set to zero.

[b] molecular constants from ref. [30] .

[c] this work, data calculated from the fitted potential energy surface of ref. [2].

[d] experimental data, ref. [14].

[e] molecular constants from ref. [19] .

[f] experimental data, this work and ref. [18].

8 Figure captions

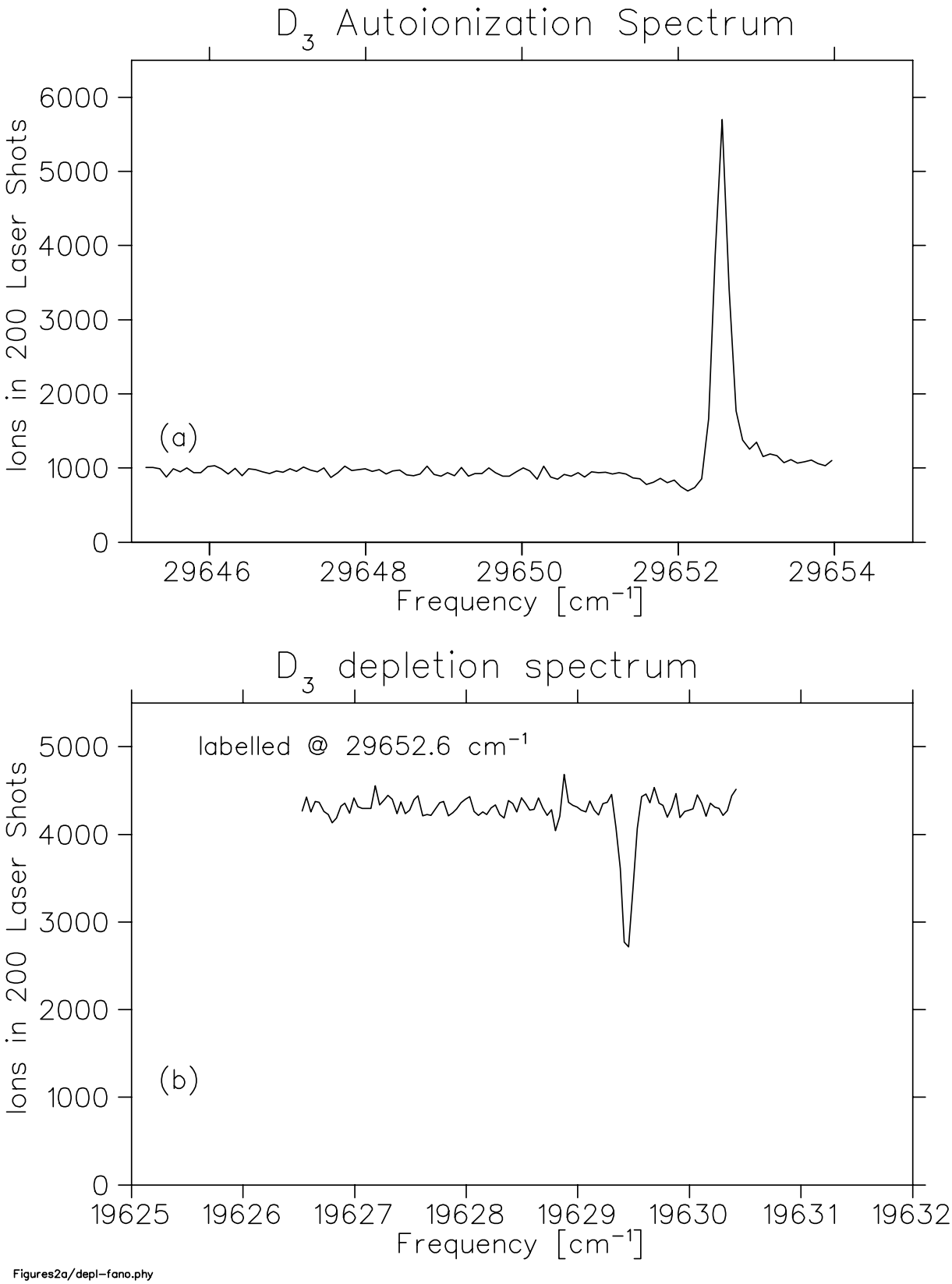

Figure 1: Depletion spectra of metastable D_3 molecules. The labelling laser was set to excite the n=39 (a) and n=40 (b) lines of the field-ionizing Rydberg series 1, respectively. The excitation laser was scanned between 17329 cm^{-1} and 17339.5 cm^{-1} (part a) in the tuning range of Rhodamine 6G, and between 19623 cm^{-1} and 19635 cm^{-1} in the tuning range of Coumarin 307 (part b).

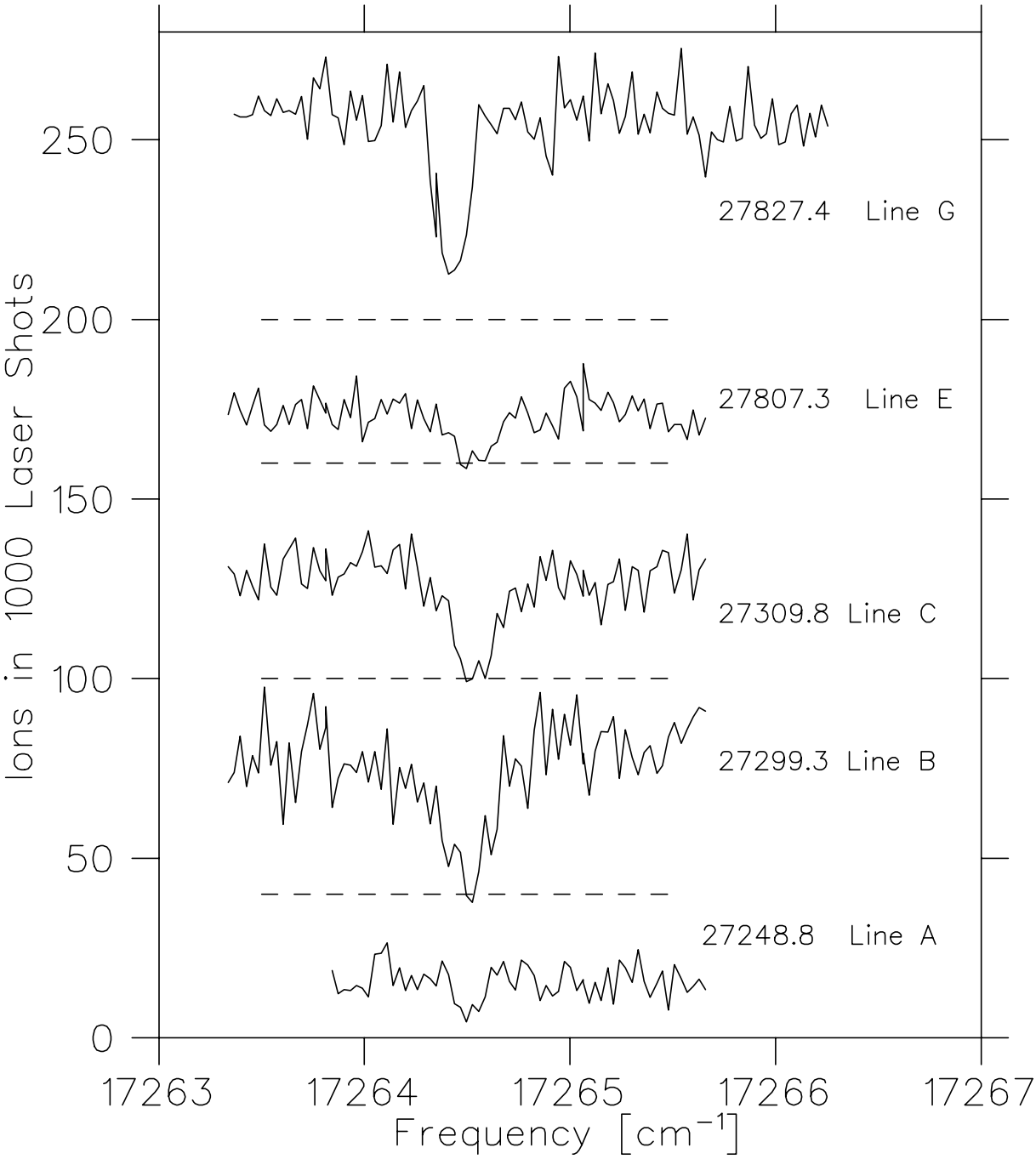

Figure 2:

(a) Fano type resonance above the first ionisation threshold of the 2p $^2A''_2(0,0,0,0)$ state of D_3.

(b) Depletion spectrum with the labelling laser set to the maximum of the Fano resonance at 29652.6 cm^{-1} . The excitation laser was operated with the dye Coumarin 307 and scanned in the 19626.5 cm^{-1} to 19630.5 cm^{-1} frequency range.

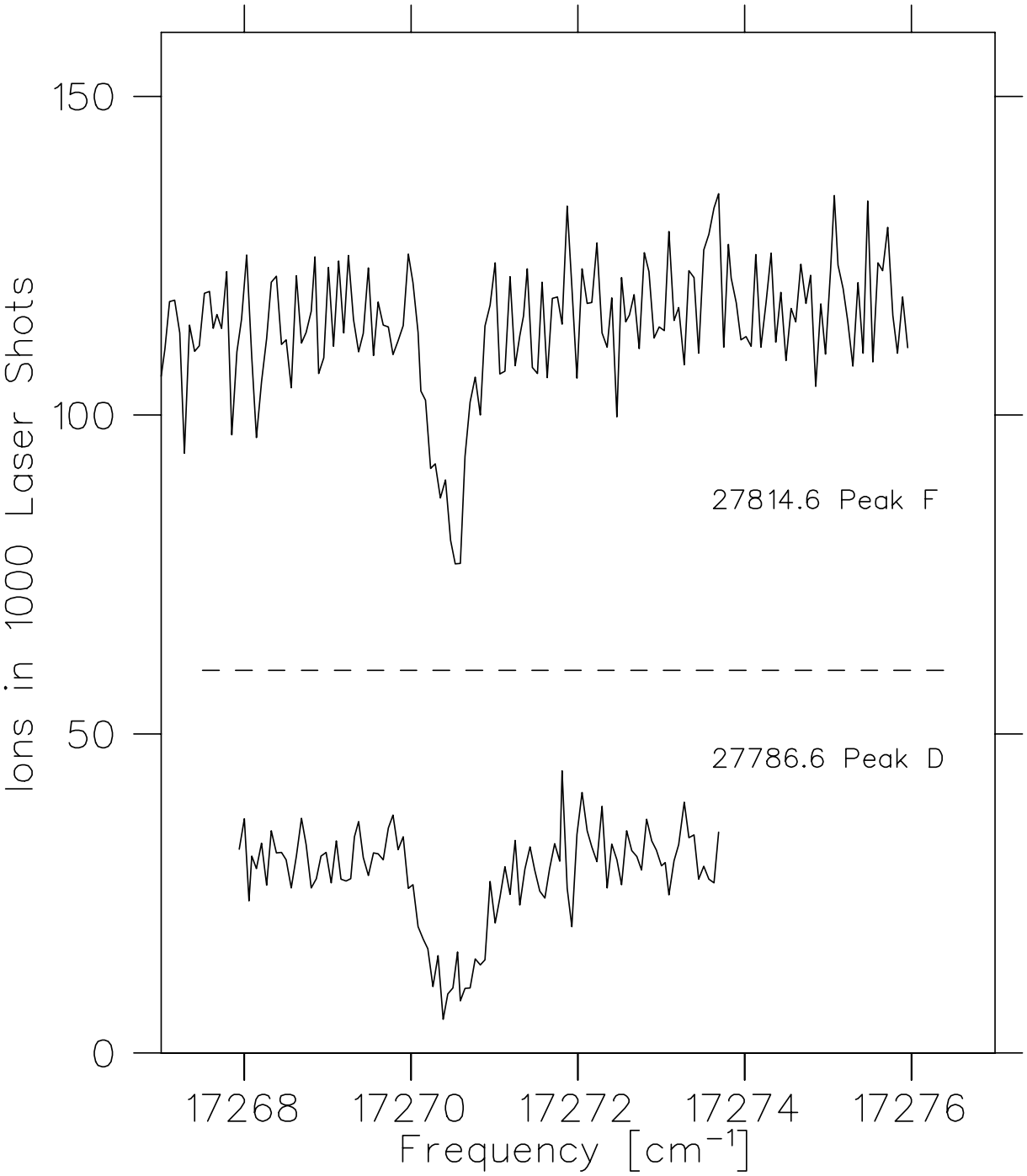

Figure 3: Autoionizing states excited by vibrationally diagonal single-photon excitation of vibrationally excited D_3 2p $^2A_2''$ molecules in the (a) 27230 cm^{-1} to 27350 cm^{-1} and the (b) 27760 cm^{-1} to 27840 cm^{-1} frequency range. The positions of the n=7 and n=8 lines of the Rydberg series 3 to 5 (see Table 1) are indicated by open circles.

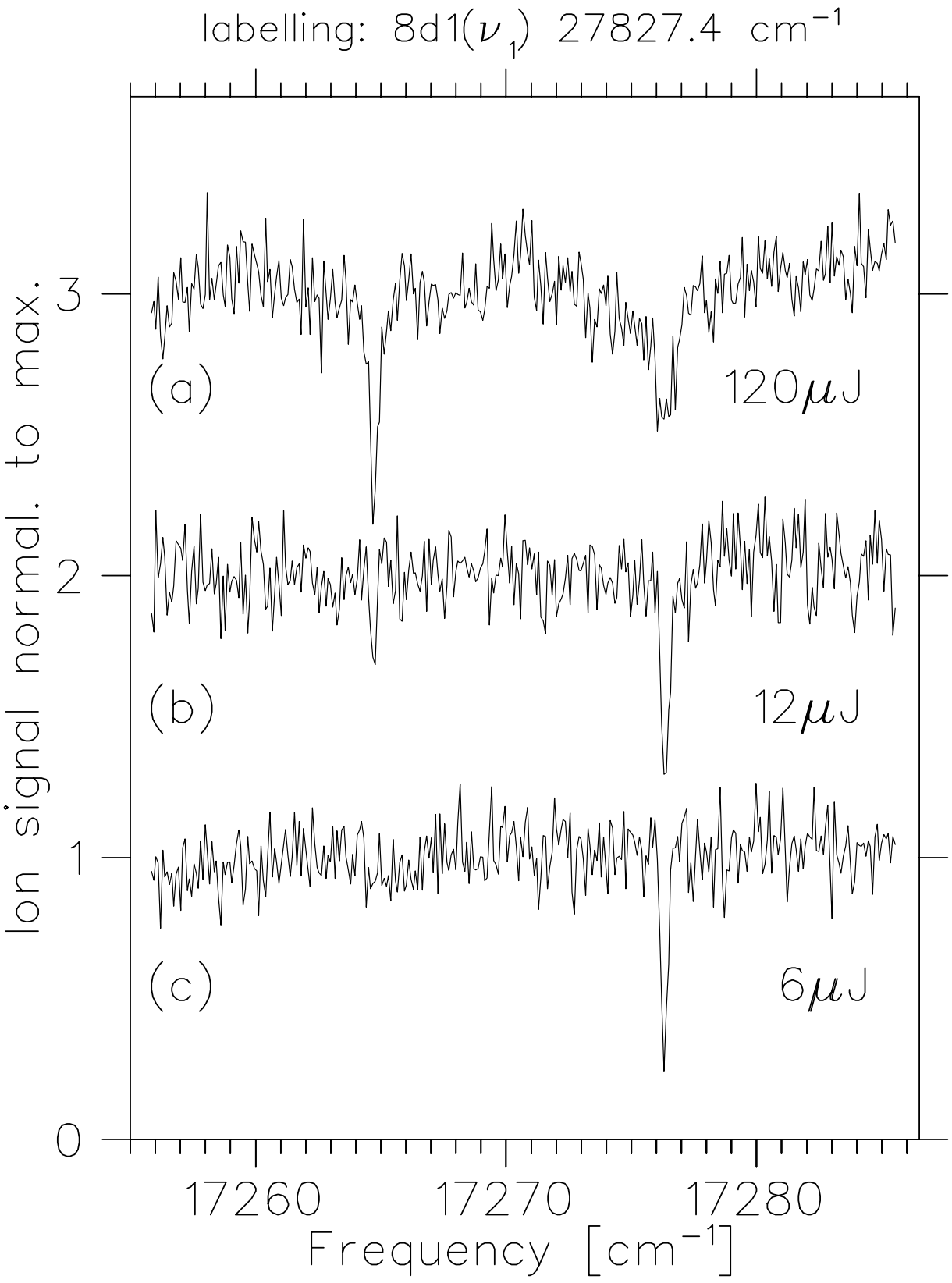

Figures2a/d3−2p10−3d−vis.phy

Figure 4: Depletion spectra with the labelling laser tuned to the peaks A,B,C,E, and G of fig. 3. The excitation laser was scanned in the 17263.5 to 17265.5 cm^{-1} spectral range. For clarity of presentation, the spectra are shifted vertically with respect to each other, and separated by a dashed line which indicates the zero-point.

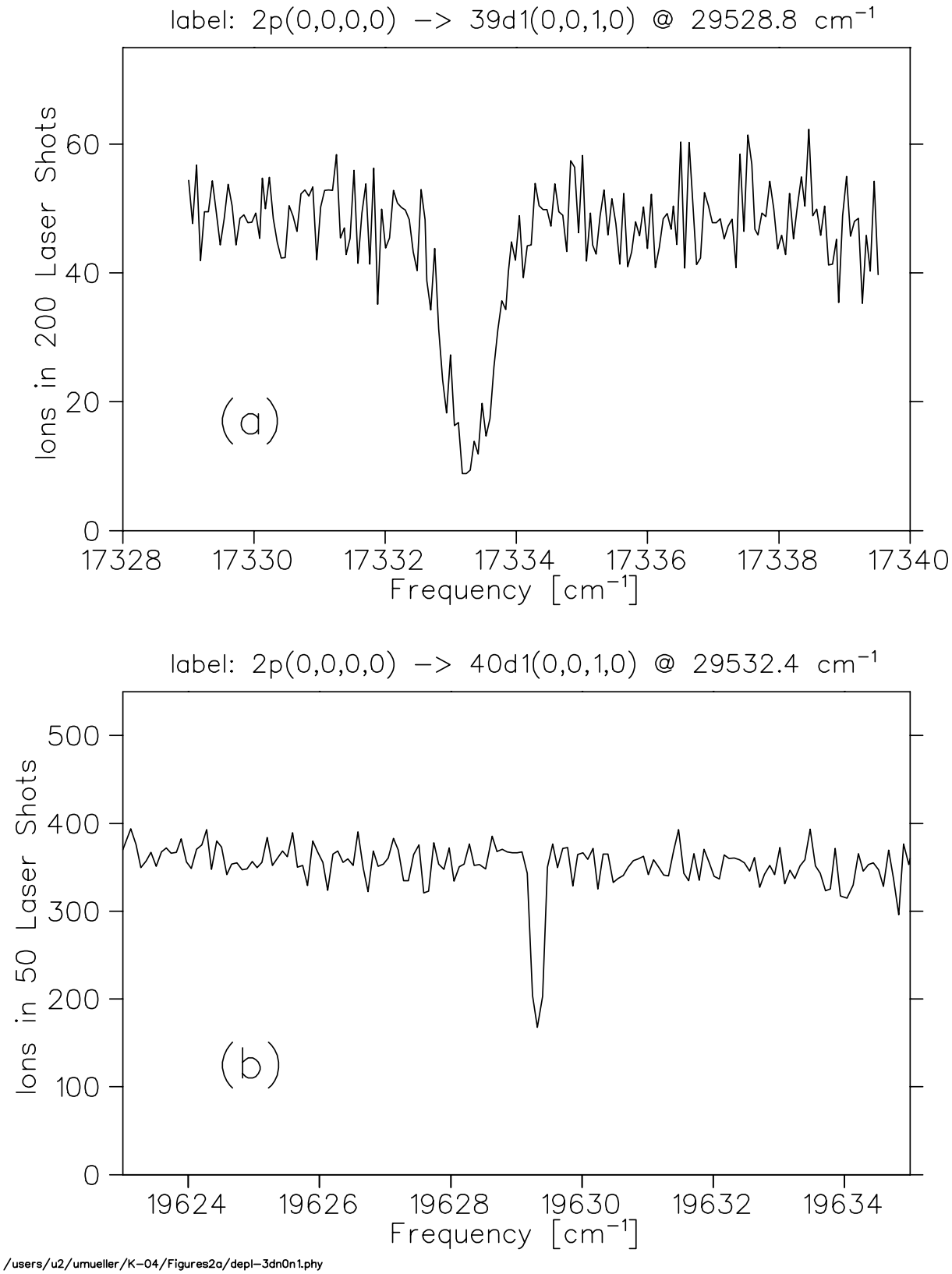

Figure 5: Depletion spectra with the labelling laser tuned to the peaks D and F of fig. 3. The excitation laser was scanned in the 17268 to 17274 cm^{-1} spectral range. For clarity of presentation, the spectra are shifted vertically with respect to each other, and separated by a dashed line which indicates the zero-point.

Figure 6: Depletion spectra with the labelling laser tuned to peak G of fig. 3. The excitation laser was scanned in the 17255 to 17285 cm^{-1} spectral range. In spectrum a, the pulse energy of the excitation laser was 120 μJ. In the spectra b and c, the excitation laser was attenuated by factors of 10 and 20 respectively using neutral density filters. The ion signal was normalized. For clarity of presentation, the curves are shifted

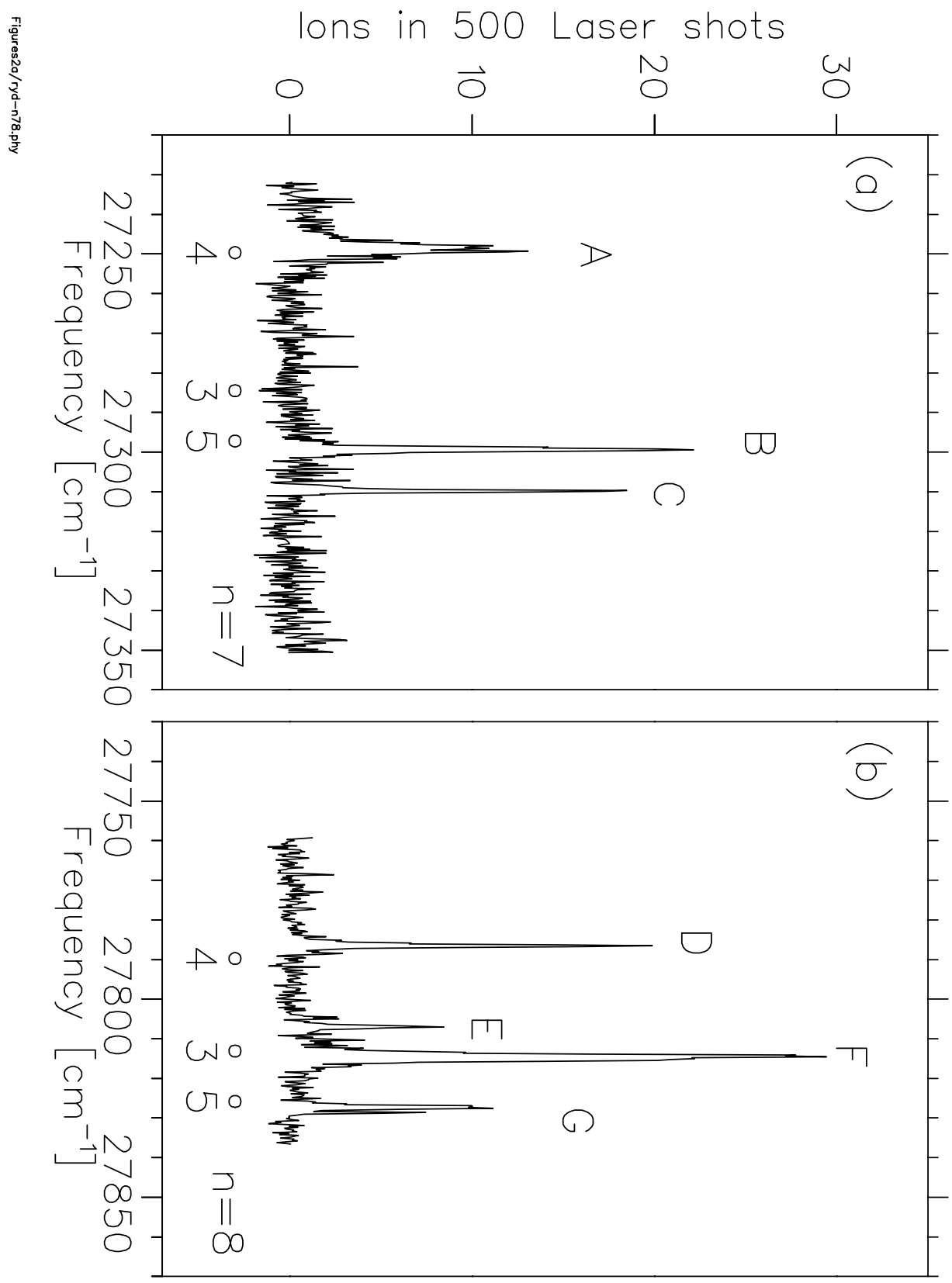

Figure 7: Level scheme containing states and transitions investigated by depletion spectroscopy in this paper. The vibrational levels are labelled by the quantum numbers (ν_1,ν_2). The ionization limits of series 3 to 5 (see Table 1) are indicated by the thin vertical lines. The pumped transitions are shown by thick vertical lines with arrowheads. Transitions in the ultraviolet range were used for labelling, those in the visible

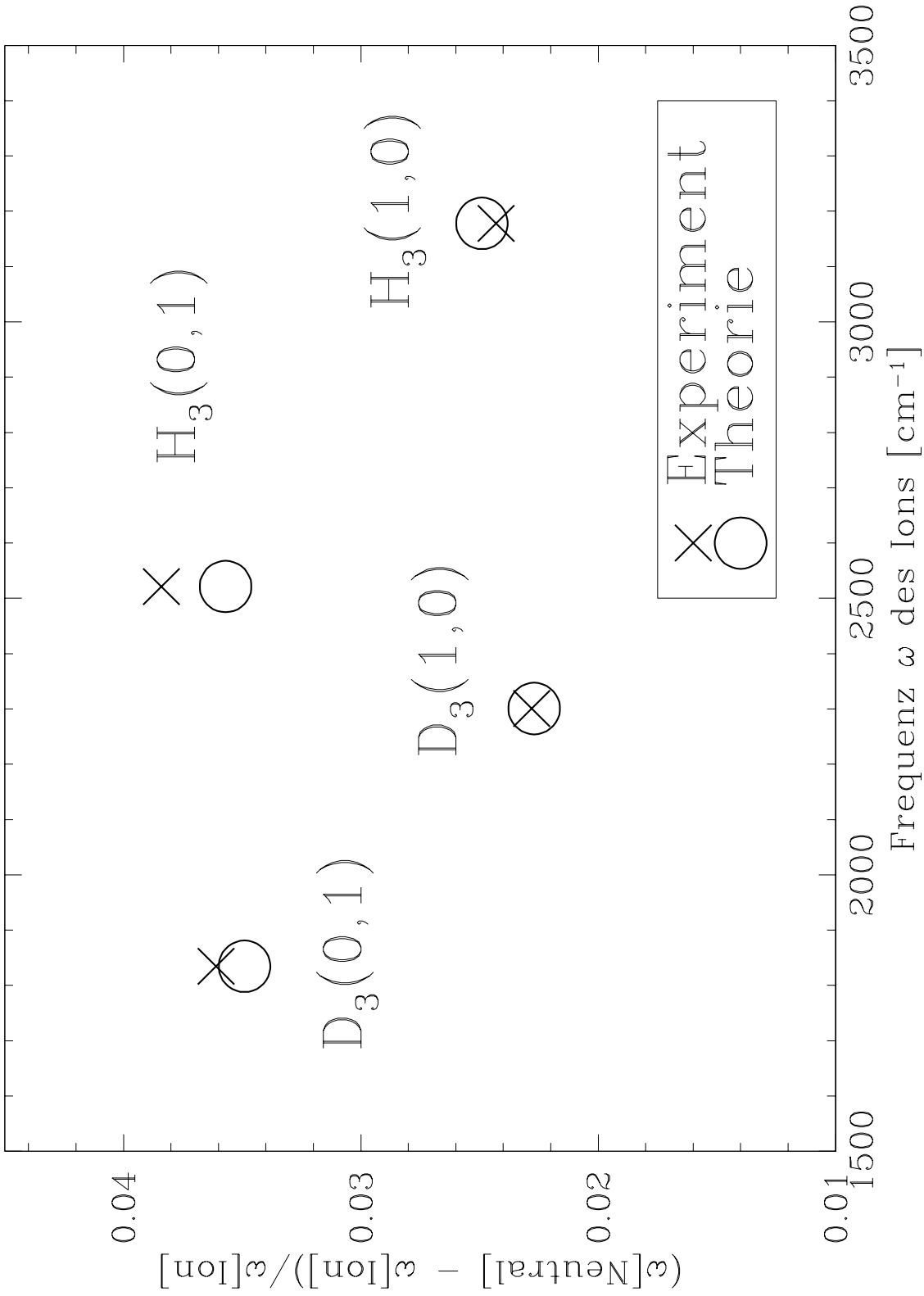

Figure 8: Differences between the vibrational frequencies of the (neutral) 2p $^2A_2''$ states of D_3 and H_3 and those of the D_3^+ and H_3^+ ions. The differences were normalized to the vibrational frequencies of the corresponding ions. The vibrational states are labelled by the quantum numbers (ν_1,ν_2).